Modeling, development, and testing of a shortwave infrared supercontinuum laser source for use in active hyperspectral imaging

Joseph Meola[a], Anthony Absi[a], James D. Leonard[a], Agustin I. Ifarraguerri[b], Mohammed N. Islam[c,d], Vinay V. Alexander[c], Jerome Zadnik[e]

[a]Air Force Research Laboratory, WPAFB, OH 45433
[b]SAIC, Arlington, VA 22203
[c]University of Michigan, Ann Arbor, MI 48109
[d]Omni Sciences, Inc., Dexter, MI 48105
[e]EOIR Technologies, Inc., Fredericksburg, VA 22408

ABSTRACT

A fundamental limitation of current visible through shortwave infrared hyperspectral imaging systems is the dependence on solar illumination. This reliance limits the operability of such systems to small windows during which the sun provides enough solar radiation to achieve adequate signal levels. Similarly, nighttime collection is infeasible. This work discusses the development and testing of a high-powered super-continuum laser for potential use as an on-board illumination source coupled with a hyperspectral receiver to allow for day/night operability. A 5-watt shortwave infrared supercontinuum laser was developed, characterized in the lab, and tower-tested along a 1.6km slant path to demonstrate propagation capability as a spectral light source.

Keywords: hyperspectral, supercontinuum, active, shortwave infrared

1. INTRODUCTION

Use of hyperspectral imaging (HSI) systems continues to grow due to their ability to passively collect spectral characteristics of materials from long ranges.[1] These spectral characteristics are then used to perform various exploitation tasks, such as material identification[2] and target detection.[3,4] Hyperspectral sensors are typically divided into classes based upon the region of the electromagnetic spectrum in which they operate. Reflective HSI systems operate in the visible through shortwave infrared (SWIR) portion of the spectrum, i.e., 0.4-2.5μm. Thermal HSI systems operate in the longwave infrared, i.e., 7.5-14μm. Additionally, there are systems that operate in the reflective-thermal crossover region in the midwave infrared (MWIR), i.e., $3-5\mu m$. Systems operating in the reflective region measure solar radiation that is reflected by objects in the scene. As such, these sensor systems can only operate during daytime in conditions where enough solar radiation exists. Systems operating in the thermal region collect radiation that is emitted or reflected by objects within the scene. As such, these systems can theoretically operate in day or night, given appropriate thermal and atmospheric conditions.

While thermal systems possess day/night operability, the sensor and detector technology is not as mature as those operating in the reflective region. Reflective HSI systems typically offer superior spatial and spectral resolution with lower noise when compared with thermal systems.[5] Additionally, key spectral characteristics used for detection/identification of various materials exist in the reflective region. Development of reflective HSI systems coupled with an on-board light source would allow for improved operability for such exploitation tasks. In theory, this system would be capable of operating not only at night, but during overcast skies and other low solar illumination conditions. Additionally, this theoretical system could simplify exploitation tasks by allowing operators to remove illumination unknowns associated with the data by utilizing the on-board source.

Broadband, high power lamps exist as potential on-board light sources for reflective HSI systems. However, these sources are difficult to collimate and direct with small divergence over long distances. Conventional lasers with high brightness and low divergence are available, but their narrow spectral bandwidth limits their utility

Algorithms and Technologies for Multispectral, Hyperspectral, and Ultraspectral Imagery XIX, edited by Sylvia S. Shen, Paul E. Lewis, Proc. of SPIE Vol. 8743, 87431D · © 2013 SPIE
CCC code: 0277-786X/13/$18 · doi: 10.1117/12.2015940

Downloaded From: http://proceedings.spiedigitallibrary.org/ on 06/03/2013 Terms of Use: http://spiedl.org/terms

as an illumination source for HSI systems. While multi-spectral systems have been developed using multiple narrowband laser sources,[6] extension to hyperspectral systems would be impractical. Super-continuum lasers (SCLs) share with conventional lasers useful characteristics such as high brightness and low divergence. However, unlike conventional lasers, SCLs possess a broad spectral bandwidth.[7] Additionally, the spectral power density of the SCL can be engineered to produce sources with power over a predefined wavelength range, providing improved energy efficiency when compared to lamp sources. With the advent and continued development of high-powered SCLs, these sources provide a candidate for use in developing a so-called "active HSI" system. A number of challenges exist with the use of SC lasers as illumination sources. Modeling of the radiative transfer process and calibration associated with the system is complicated by the spectral dependence of laser divergence properties. Additionally, atmospheric turbulence effects must be mitigated. Recent work using a visible to near infrared SCL has demonstrated potential as an illumination source and has also illustrated several of the challenges mentioned here.[8]

Omni Sciences, Inc.,[9] in conjunction with the University of Michigan (UM), has developed a number of high-powered SC lasers operating in a number of different wavelength regions. They have recently developed a 5W, shortwave infrared SC prototype operating from $1.5 - 2.4\mu m$. The system's characteristics (beam divergence, beam quality, spectral power density) were measured in a laboratory setting. To demonstrate its potential as a broadband SWIR illumination source at longer ranges, the SC laser was then placed in a tower and directed along a 1.6km slant path to illuminate various target materials. A broadband SWIR camera along with a spectral radiometer were placed near the target materials at ground level to measure the reflected laser illumination. In Section 2, a brief discussion of the SWIR SCL (SSCL) is given. In Section 4, the tower test experiments are outlined in detail and the results discussed. Finally, in Section 5, a summary is provided along with discussion of on-going and future work in this area.

2. SUPERCONTINUUM LASER

Omni Sciences, Inc. and UM have developed a 5W SWIR SCL (SSCL) operating from $1.5 - 2.4\mu m$. Basic information about the laser and its characteristics are provided here.

2.1 Laser development

The block diagram for the 5W SSCL is shown in Figure 1, which consists of an amplified 1.54μm laser source followed by a spectrum shifting fused silica fiber. The amplified 1.54μm laser source consists of a 1542nm seed laser diode that is driven by electronic circuits to provide a 0.5 ns pulse at variable repetition rates from 20 MHz down to a few KHz. The pulses are amplified by two stages of Erbium-Ytterbium-based fiber amplifiers (EYFA) designated as the pre-amplifier and the power-amplifier, respectively. The pre-amplifier uses a 2m length of 12/130 micron (core/cladding diameter) EYFA, and the power amplifier consists of a 7m length of 12/130 micron (core/cladding diameter) EYFA pumped by a 25W, 940nm diode. A 100GHz band pass filter is used after the pre-amplifier to filter out the amplified spontaneous emission. The amplified 1540nm light is spliced onto 10m length of 8/125 micron (core/cladding diameter), 0.125 NA, PM1550 fiber, which generates the SC through the interplay of various non-linear phenomena, such as modulation instability, stimulated Raman scattering, etc. The final SC output is then collimated using a gold-coated parabolic mirror to produce a collimated beam with a diameter of 6.5 mm. Further information on the SCL technology can be found in the authors' references.[10]

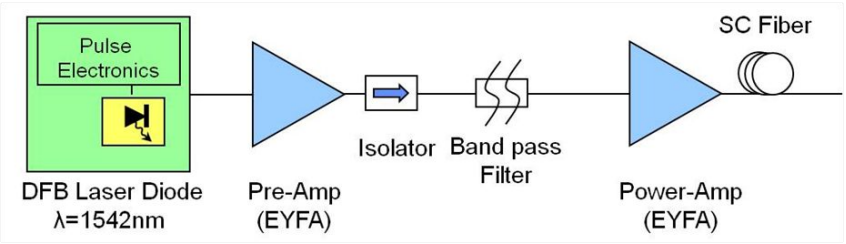

Figure 1: Block diagram for 5W shortwave supercontinuum laser

Downloaded From: http://proceedings.spiedigitallibrary.org/ on 06/03/2013 Terms of Use: http://spiedl.org/terms

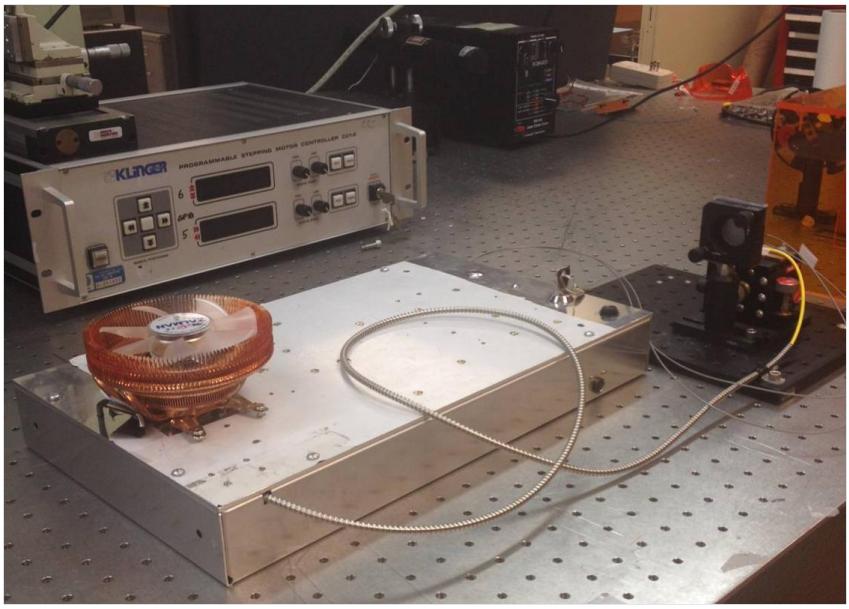

Figure 2: 5W shortwave supercontinuum laser

2.2 Laboratory characterization

The output power of the SSCL was measured in the lab at UM. The total integrated power of the laser was measured as 5.03W using a thermal power meter with a collimating mirror (5.1W without mirror). The spectral power density was measured using a monochromator with the laser as the input source and an Indium-Galium-Arsenide (InGaAs) detector at the output slit. The measured spectrum was corrected for the spectral response of the InGaAs detector to provide a true measure of the spectral power density. Figure 3 displays the measured spectral power density for the 5W laser source. The full-angle beam divergence is approximated using the

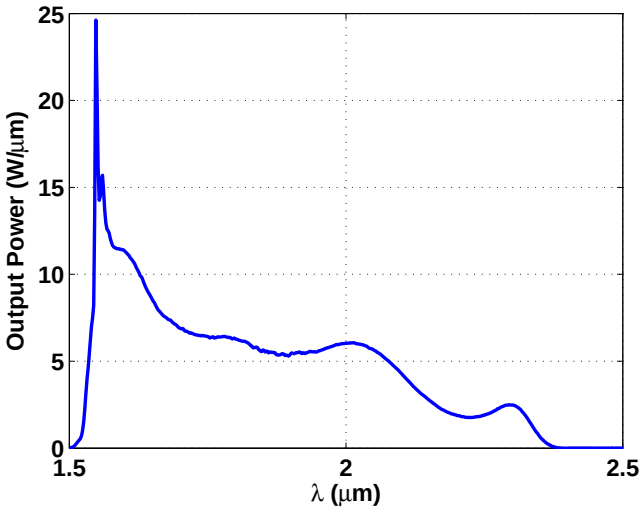

Figure 3: Laser spectral power density

measured spot size at 2.0μm and is found to be approximately 0.5mrad.

Downloaded From: http://proceedings.spiedigitallibrary.org/ on 06/03/2013 Terms of Use: http://spiedl.org/terms

3. RADIOMETRIC MODELING

In order to effectively predict the SSCL performance as a candidate illumination source for coupled use with HSI receivers, an accurate radiometric model must be developed. The modeling is complicated by both the wavelength dependence of the laser characteristics and by atmospheric turbulence. A preliminary model for estimating surface irradiance, pupil-plane radiance, and signal-to-noise is provided here.

3.1 Super-continuum laser propagation

Conventional lasers are considered near monochromatic. A laser is specified by a full-angle beam divergence θ from which the laser spot diameter in the far-field d is approximated by,

$$d \approx \theta * R \tag{1}$$

where R is the range to the target. The spot diameter is defined assuming Gaussian laser beam propagation. Defining the half-angle beam divergence as,

$$\phi = \theta/2 \tag{2}$$

the laser beam waist is given by,

$$w_0 = \frac{\lambda}{\pi\phi} \tag{3}$$

where λ is the center wavelength of the laser. The propagating Gaussian laser beam field is given by,[11,12]

$$\tilde{E}\left(x,y,z,t\right) = \tilde{E}_0(z)e^{-\frac{x^2+y^2}{w^2(z)}} \times \text{phase} \tag{4}$$

where z is the propagation dimension, (x,y) are the transverse field dimensions, t is time, $w(z)$ is the laser spot radius as a function of range given by,

$$w^2(z) = w_0^2\left[1+\left(\frac{\lambda z}{\pi w_0^2}\right)^2\right] \tag{5}$$

and $\tilde{E}_0$ is given by,

$$\tilde{E}_0(z) = \sqrt{\frac{2}{\pi}}\frac{1}{w(z)}\sqrt{P_0} \tag{6}$$

where P_0 is the output power of the laser. The irradiance distribution (power distribution) of the laser at distance z is then specified by,

$$E(x,y,z) = \left|\tilde{E}\left(x,y,z,t\right)\right|^2 = \tilde{E}_0^2(z)e^{-2\frac{x^2+y^2}{w^2(z)}} \tag{7}$$

The total incident irradiance for an area $A(x,y)$ at distance z can then be calculated by integration over the area as,

$$E_{tot}\left(A(x,y),z\right) = \iint\limits_{A(x,y)} E(x,y,z)dxdy \tag{8}$$

Often, the fractional irradiance incident on a circular area of radius a is computed,

$$E_{frac}(r=a,z) = 1 - e^{-2a^2/w^2(z)} \tag{9}$$

where $r^2 = x^2+y^2$. From this, one determines that the fractional power contained in a circle with radius equal to the spot size radius $w(z)$ is equal to $1-e^{-2}$ or about 86%. The irradiance distributions above do not take into account power loss from atmospheric absorption over the laser-to-target path, $\tau_L(z,\lambda)$, i.e., lossless transmission.

For SCLs, the monochromatic assumption no longer holds as λ no longer represents the center wavelength of an extremely narrowband but rather a relatively broad wavelength band. Consequently, the beam divergence and resulting spot size parameters must be modeled with a wavelength dependent. The wavelength dependence

Downloaded From: http://proceedings.spiedigitallibrary.org/ on 06/03/2013 Terms of Use: http://spiedl.org/terms

is observed in the beam waist equation given in (3). The spot diameter at two different wavelengths will vary by the ratio of those wavelengths. To make the wavelength dependence in the irradiance calculations more explicit, a wavelength parameter is added to the previously derived equations $w_0 = w_0(\lambda)$, $w(z) = w(z,\lambda)$, $\tilde{E}_0(z) = \tilde{E}_0(z,\lambda)$, $P_0 = P_0(\lambda)$, and $E(x,y,z) = E(x,y,z,\lambda)$. The total and fractional irradiance calculations are now a function of wavelength.

3.2 Pupil-place radiance

For the SSCL tower test, both a broadband camera and a spectral radiometer are used to measure the laser characteristics. The broadband camera is responsive to illumination over a wavelength range of 1-5μm. As a result, both reflected and thermally emitted radiation contribute to the total radiance measured by the camera. A simplified model[5] describing the spectral radiance reaching the broadband camera apearture is given by,

$$\begin{aligned} L(\lambda) = {} & \tfrac{E(\lambda)}{\pi}\tau_L(\lambda)\tau(\lambda)\rho(\lambda) + \tfrac{E_{sun}(\lambda)}{\pi}\tau(\lambda)\rho(\lambda) + L_d(\lambda)\tau(\lambda)\rho(\lambda) + \big(1-\rho(\lambda)\big)L_{BB}(\lambda,T)\tau(\lambda) \\ & + L_p(\lambda) + L_{atm,d}(\lambda)\rho(\lambda)\tau(\lambda) + L_{atm,u}(\lambda) \end{aligned} \tag{10}$$

where E is the lossless spectral irradiance of the laser on the target surface (location specified by x, y, z), E_{sun} is the solar spectral irradiance on the target surface, ρ is the target spectral reflectance, τ is the atmospheric transmission along the target-to-sensor path, τ_L is the atomspheric transmission along the laser-to-target path, L_d is the diffuse solar downwelling radiance, L_p is the solar path radiance, L_{BB} is the blackbody function with target temperature T, $L_{atm,d}$ is the thermal downwelling radiance produced by the atmosphere, and $L_{atm,u}$ is the thermal path radiance. Note that for an operational system, the laser and receiver would most likely be on the same platform resulting in equivalent transmission terms, i.e., $\tau_L = \tau$. The majority of the tower test was performed at night for which the solar terms of the model can be ignored resulting in,

$$L(\lambda) = \tfrac{E_L(\lambda)}{\pi}\tau(\lambda)\rho(\lambda) + \big(1-\rho(\lambda)\big)L_{BB}(\lambda,T)\tau(\lambda) + L_{atm,d}(\lambda)\rho(\lambda)\tau(\lambda) + L_{atm,u}(\lambda) \tag{11}$$

where

$$E_L(\lambda) = E(\lambda)\tau_L(\lambda) \tag{12}$$

This model provides a starting point for predicting laser performance. However, this model does not incorporate the impact of atmospheric turbulence, which plays an important role in laser propagation as will be shown in the tower test results. Additionally, laser backscatter radiance is not included here, which may play a significant role for a coupled laser-HSI system. These terms should be included in future modeling work.

3.3 Theoretical signal to noise ratio

Using the pupil-place radiance model, the expected signal-to-noise ratio (SNR) for the broadband camera used during the field test can be modeled.[5] For these applications, the "signal" is the reflected laser illumination,

$$L_s(\lambda) = \frac{E_L(\lambda)}{\pi}\tau(\lambda)\rho(\lambda) \tag{13}$$

and the background is the total pupil-plane radiance,

$$L_b(\lambda) = L(\lambda) \tag{14}$$

which includes undesired thermal emission from both the atmosphere and targets. The focal plane spectral irradiance for the signal and background are approximated by,

$$\begin{aligned} E_s(\lambda,\theta_c) &= \tfrac{\pi K(\theta_c)}{4(f/\#)^2+1}\tau_o(\lambda)L_s(\lambda) \\ E_b(\lambda,\theta_c) &= \tfrac{\pi K(\theta_c)}{4(f/\#)^2+1}\tau_o(\lambda)L_b(\lambda) + E_o(\lambda,\theta_c) \end{aligned} \tag{15}$$

where K represents the irradiance roll-off for field angle θ_c for the system, τ_o is the transmission of the warm optics, and E_o is the irradiance due to veiling glare, stray radiance, and instrument self emission. This term can be approximated as,

$$E_o(\lambda) = \frac{4\pi(f/\#)^2}{4(f/\#)^2+1}L_{BB}(\lambda,T_c) + \big[1-\tau_o(\lambda)\big]\tau_c(\lambda)\frac{\pi}{4(f/\#)^2+1}L_{BB}(\lambda,T_o) \tag{16}$$

Downloaded From: http://proceedings.spiedigitallibrary.org/ on 06/03/2013 Terms of Use: http://spiedl.org/terms

where T_c is the temperature of the cold shield, T_o is the temperature of the warm optics and where the impact of field angle θ_c is considered negligible.

Using the focal plane irradiance, the number of detected photoelectrons is estimated. The photon arrival/detection is a random process, therefore, the number of detected photoelectrons for the signal, N_s and for the background N_b are both random processes. The mean detected photoelectrons for the signal and background for integration time t_d is estimated by,

$$\begin{aligned} \mu_s &= E\{N_s\} = A_d t_d \int \tfrac{\lambda}{hc}\eta(\lambda)E_s(\lambda)d\lambda \\ \mu_b &= E\{N_b\} = A_d t_d \int \tfrac{\lambda}{hc}\eta(\lambda)E_b(\lambda)d\lambda \end{aligned} \tag{17}$$

where A_d is the detector area, η is the detector quantum efficiency, and where $E\{\}$ represents expected value. The total mean number of detected photoelectrons is given by,

$$\mu_N = \mu_b + \mu_d \tag{18}$$

where μ_d is the mean number of dark current photoelectrons. The signal-to-noise ratio is given by,

$$SNR = \frac{\mu_s}{\sigma_n} \tag{19}$$

where σ_n is the noise standard deviation. This noise term can be broken up into three dominant sources,

$$\sigma_n = \sqrt{\sigma_{shot}^2 + \sigma_{dark}^2 + \sigma_{read}^2} \tag{20}$$

where σ_{shot} is the shot noise, σ_{dark} is the dark current shot noise, σ_{read} is the electronic read noise.[13] The shot noise and dark current shot noise variances are given by,

$$\begin{aligned} \sigma_{shot}^2 &= \mu_b \\ \sigma_{dark}^2 &= \mu_d \end{aligned} \tag{21}$$

While other noise sources typically exist, the shot, dark, and electronic noise are assumed to be the most dominant for these applications.

The detected photoelectrons are modeled as a random process given by,

$$N = \mu_N + \nu \tag{22}$$

where μ_N is the mean number of detected photoelectrons as defined earlier and ν is zero-mean noise with variance σ_n^2. Ideally, one would like to use a calibrated, SWIR-only camera to measure laser performance. However, a SWIR-only camera was not available at the time of the test. As a result, in order to characterize laser performance alone, the emissive portion of the signal reaching the sensor must be removed. This is accomplished by collecting data with the laser source on and laser source off and subtracting the two. The differential data is given by,

$$\Delta N = N_{on} - N_{off} = \mu_s + \tilde{\nu} \tag{23}$$

where $\tilde{\nu}$ is the combined noise source with variance given by,

$$\tilde{\sigma}_n^2 = \sigma_{n,on}^2 + \sigma_{n,off}^2 \tag{24}$$

where

$$\sigma_{n,on}^2 = \sigma_n^2 = \mu_b + \mu_d + \sigma_{read}^2 \tag{25}$$

and

$$\sigma_{n,off}^2 = \mu_{b,thermal} + \mu_d + \sigma_{read}^2 \tag{26}$$

where $\mu_{b,thermal}$ is the thermal shot noise. Ideally, one would like to remove the thermal shot noise contribution to estimate laser SNR, but this is difficult to achieve. Assuming the reflected laser illumination and emitted background radiation are similar in magnitude, $\sigma_{n,off}^2$ is used as the estimated noise variance for SNR calculations. In this case, the SNR is given by,

$$SNR = \frac{\mu_s}{\sigma_{n,off}}. \tag{27}$$

Downloaded From: http://proceedings.spiedigitallibrary.org/ on 06/03/2013 Terms of Use: http://spiedl.org/terms

4. TOWER TESTING

Tower-based testing of the 5W SSCL was performed to assess beam propagation characteristics of the laser and to demonstrate spectral reflectance retrieval capabilities. A summary of the tower test and results is provided here.

4.1 Test overview

The tower-test occurred at Wright Patterson Air Force Base (WPAFB) from 10-12 September 2012 with participation by Omni Sciences, UM, AFRL, SAIC, and EOIR Technologies. The majority of testing occurred after sunset to remove any solar contribution to the measured signal. For these tests, the SSCL was placed in a tower and directed along a slant path to a target panel on the ground. Figure 4 provides a sideview diagram of the tower-based test. The target panel consists of a plywood stand for placement/holding of the target materials

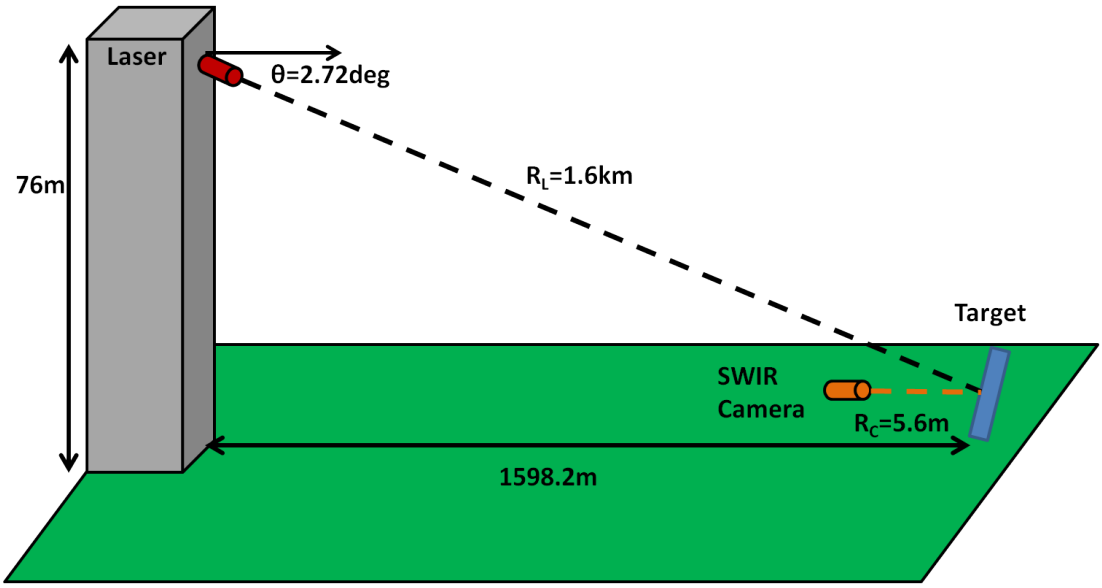

Figure 4: Diagram of tower-based test

used during the collection. The materials used include Tyvek, clear plastic drop-cloth, black and gray silt cloth, a blue tarp, white fabric, wallboard, plywood, and gray painted plywood. The stand is tilted slightly to create a normal surface with respect to the laser beam propagation angle (2.72°). The broadband camera was placed near the target panel to measure the reflected laser illumination for characterizing beam shape and SNR. In this diagram, the laser range R_L is determined by the slant range from the tower (1.6km). The SWIR camera range R_C was around 5.6m. In addition to the SWIR camera, an Analytical Spectral Devices (ASD) spectral radiometer was utlized to measure reflected spectral radiance and to demonstrate reflectance retrieval capability using the laser as a source. The spectral radiometer was placed approximately 2m from the target around 30° off normal. Figure 5 provides a diagram of the overhead layout of both the camera and spectral radiometer with respect to the target panel. Other relevant laser and camera specifications for the tower test are provided in Table 1. Note that due to power loss from the use of mirrors to direct the laser beam from the tower, the effective laser power is 4.65W rather than the lab measured 5.1W.

4.2 Beam profile and radiometric analysis

The beam propagation characteristics examined here include both the beam shape and the spectral radiance reaching the target. While a number of target materials were used during testing, the results for the Tyvek material are displayed here as this material possesses both high reflectance and strong spectral features. The laser beam shape/profile is compared with the theoretical distribution assuming Gaussian beam propagation as given in (7). Figure 6 displays the average camera output with the laser both on and off for the Tyvek material.

Downloaded From: http://proceedings.spiedigitallibrary.org/ on 06/03/2013 Terms of Use: http://spiedl.org/terms

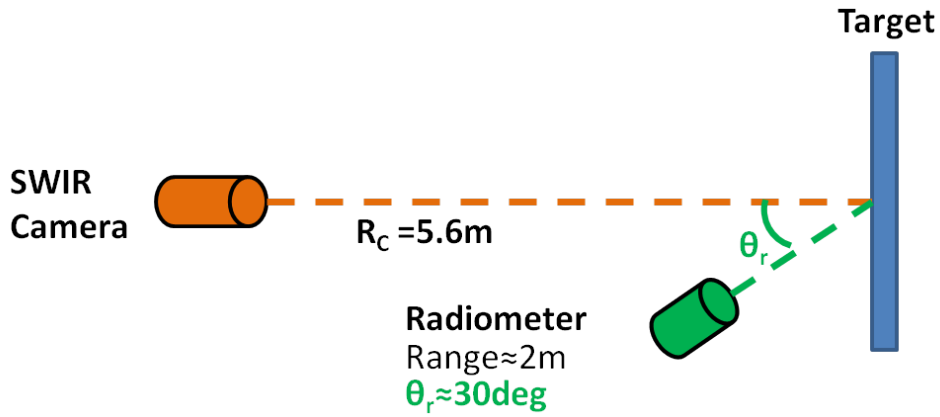

Figure 5: Overhead diagram sensor/target layout

R_L(km)	1.6
Output Power (W)	4.65
Full-angle divergence @ 2μm (mrad)	0.5
Spot size @ 2μm (m)	0.8
R_C(m)	5.6
IFOV (mrad)	0.6
GSD (cm)	0.34
FOV (m)	1.72×2.15m

Table 1: Relevant specifications for tower test

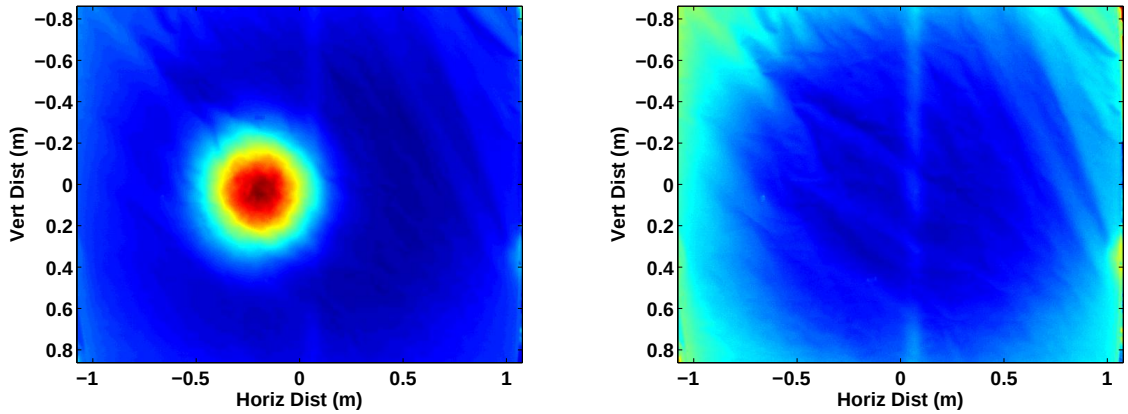

(a) Laser + background **(b) Background**

Figure 6: 1000 frame average of Tyvek panel with and without laser illumination. Camera operated with 4ms integration time.

The average is taken over 1000 frames using a 4ms integration time. The average thermal background term is subtracted to display the laser contribution alone. Figure 7 compares the measured laser distribution with the theoretical distribution. Upon visual inspection, the measured and theoretical distributions agree strongly. The measured vertical and horizontal profiles are fit to the expected exponential profile by optimizing for the laser spot radius $w(z)$ and an offset term. The measured and fit are both compared with the theoretical profile assuming a laser divergence of 0.5mrad. The estimated spot radius for the horizontal and vertical profiles are $w_x(z) = 0.38$m and $w_y(z) = 0.40$m respectively, both of which agree with the theoretical spot radius of 0.4m. Note that the spot radius and divergence vary as a function of wavelength. The profiles and parameters discussed here would be an average over the operating wavelength range due to the use of a broadband camera.

Downloaded From: http://proceedings.spiedigitallibrary.org/ on 06/03/2013 Terms of Use: http://spiedl.org/terms

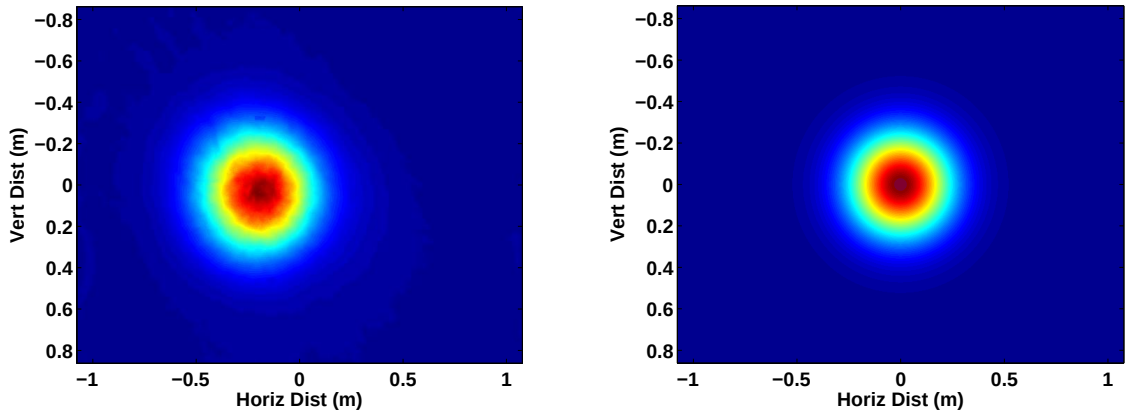

(a) Measured laser component **(b) Theoretical laser component**

Figure 7: Comparison of measured laser component on Tyvek panel with theoretical distribution

Consequently, these average values would be close the values expected at 2.0μm.

In addition to the beam shape/profile, the spectral radiance reflected from the Tyvek material is measured using the spectral radiometer and compared with the expected spectral radiance. The spectral reflectance of the Tyvek target is measured using the spectral radiometer in conjunction with a calibrated white reference material to serve as reflectance "truth". This reflectance truth is used with the laboratory measured spectral power density of the laser given in Figure 3 along with the estimated atmospheric transmission as produced by the atmospheric modeling tool MODTRAN[14] to predict the spectral radiance at the camera aperture. The estimated atmospheric transmission along the laser-to-target path (τ_L) with length R_L and transmission along the target-to-camera path (τ) with length R_C are shown in Figure 8. Figure 9 compares the theoretical spec-

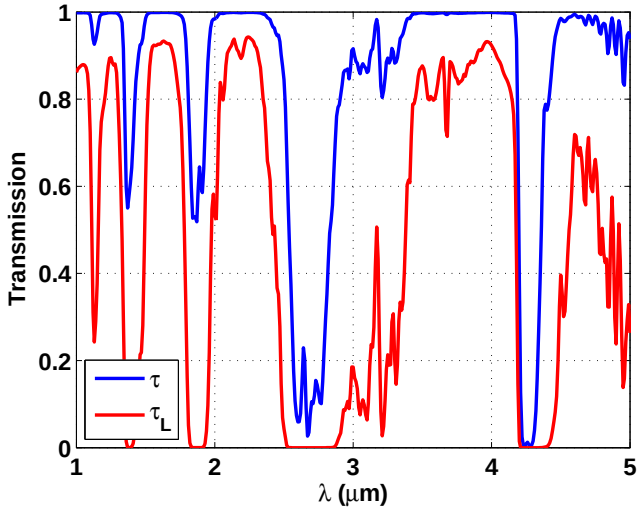

Figure 8: Estimated atmospheric transmission over sensor-to-target and laser-to-target paths for tower-based test

tral radiance with that measured by the spectral radiometer. Strong agreement exists between the measured and theoretical spectral radiance for the Tyvek material. Differences exist near the laser pump wavelength of 1.55μm that may result from differences in the spectral resolution of the laboratory monochromator and spectral radiometer.

Downloaded From: http://proceedings.spiedigitallibrary.org/ on 06/03/2013 Terms of Use: http://spiedl.org/terms

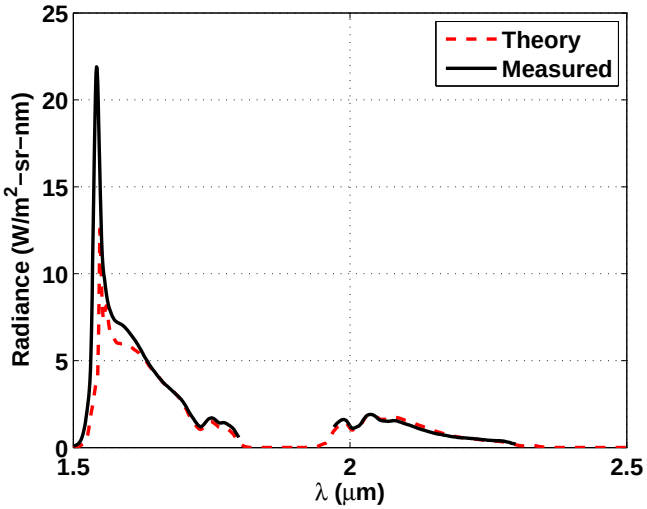

Figure 9: Comparison of measured and theoretical pupil-plane radiance for tyvek

In addition to the measured spectral radiance, the SNR is computed using the broadband camera measurements. The average laser output with background emission subtracted is used as the signal μ_s. The variance of the background measurements is used as the noise term σ_n^2. The average SNR within the laser spot size is 80.17, which is significantly less than the predicted SNR of 236.8 based upon the predicted pupil-plane radiance and the camera characteristics. Since the measured and theoretical pupil-plane spectral radiance are similar, this SNR difference is most likely related to model mismatch between the theoretical and actual camera performance, non-Lambertian target materials, or atmospheric turbulence. More testing of the camera is required to determine this. Atmospheric turbulence acts as an additional noise term that must be accounted for when trying to predict operational performance of the SSCL. Figure 10 displays the single frame camera output with laser illumination as opposed to the 1000 frame average shown earlier. Atmsopheric turbulence in the form of

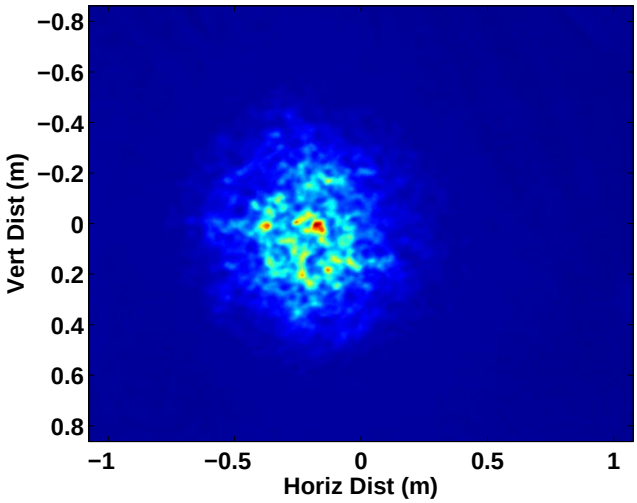

Figure 10: Illustration of turbulence effect (scintillation) on propagated laser beam

scintillation is evident in the imagery. Accordingly, a turbulence term must be included in future modeling of the system in order to better predict performance.

Downloaded From: http://proceedings.spiedigitallibrary.org/ on 06/03/2013 Terms of Use: http://spiedl.org/terms

4.3 Reflectance retrieval

The spectral radiometer was additionally used to perform spectral reflectance retrieval of the target materials using the tower-based laser as the illumination source. This test is used to determine if the laser provides enough signal across the spectral bands of interest to retrieve spectral reflectance information from targets. The spectral radiometer was positioned as demonstrated in Figure 5. In order to perform reflectance retrieval using the spectral radiometer, a spectrally-flat white reference material is required. A large 2'x2' piece of Spectralon® was used as the white reference. This sample was held in place on the plywood stand in order to collect the white reference at the same illumination/viewing angle as the target measurement. The retrieved reflectance of several target materials is shown below in comparison with lab reflectance collected earlier. The majority of retrieved reflectance curves agree closely with the lab truth, especially with respect to spectral shape of the curves. For many of the materials, a reflectance offset exists between the truth and the retrieved reflectance. This most likely results from non-Lambertian target surfaces and differences that exist between illumination/viewing geometry for the lab and field measurements.

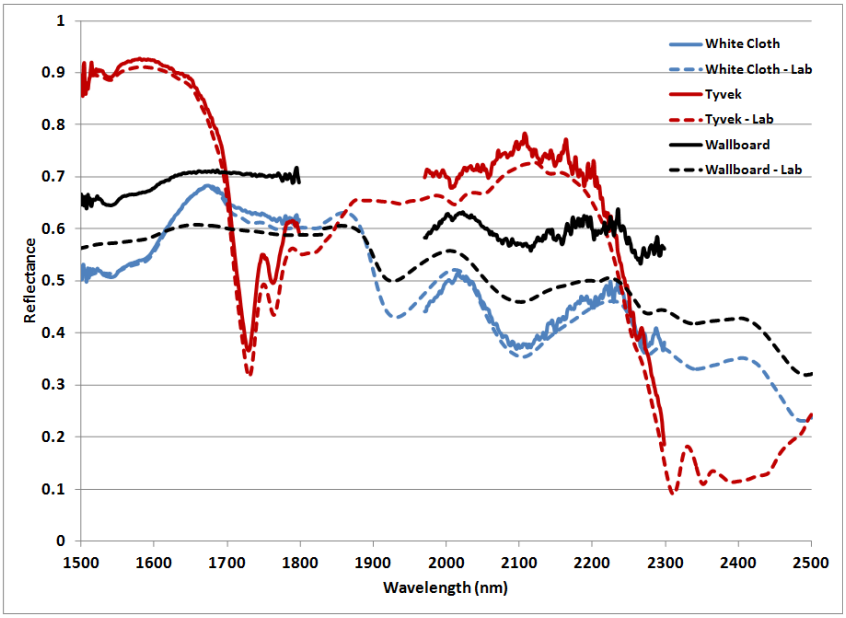

Figure 11: Retrieved reflectance of white cloth, tyvek, and wallboard

5. CONCLUSION AND FUTURE WORK

A recently developed high powered, shortwave infrared super-continuum laser was discussed here in the context of use as a potential illumination source for an active HSI system. The 5W SSCL was characterized in a laboratory and tower tested to demonstrate its operating characteristics. Additionally, a model for predicting propagation and radiometric performance was provided. The results of the tests demonstrate proof-of-concept for use of the laser as an illumination source and for reflectance retrieval of various target materials. Additionally, the tower test served as model validation with strong agreement between the modeled and measured pupil-plane radiance. The results of the tower test provided insight into the challenges of using the SSCL as an illumination source, which include signal degradation due to atmospheric turbulence and the necessity to use relatively small laser spot sizes to ensure adequate signal levels.

Omni Sciences, Inc. and UM are currently in the process of developing a 25W SSCL operating over $1.95-2.55\mu$m. Future work will include potential tower testing of this unit with a SWIR HSI receiver to demonstrate the full active HSI concept. Additionally, further work is required to develop a more acccurate and realistic system model, which will include atmospheric turbulence and other relevant radiative transfer terms.

Downloaded From: http://proceedings.spiedigitallibrary.org/ on 06/03/2013 Terms of Use: http://spiedl.org/terms

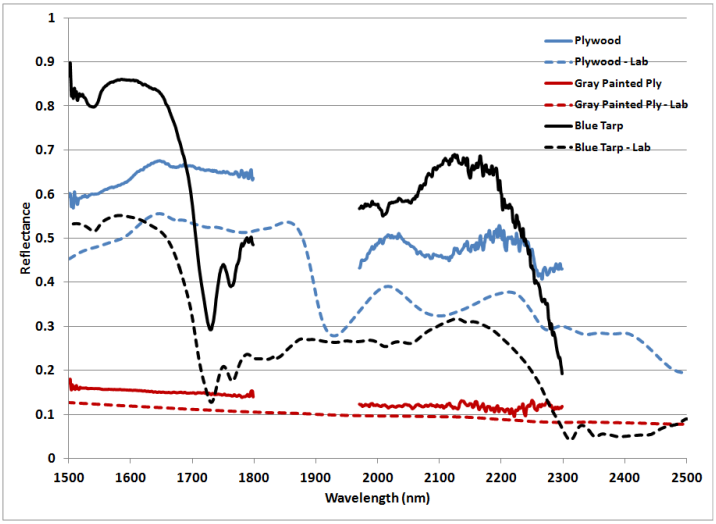

Figure 12: Retrieved reflectance of plywood, gray painted plywood, and blue tarp

REFERENCES

1. B. Stevenson, R. O'Connor, W. Kendall, A. Stocker, W. Schaff, D. Alexa, J. Salvador, M. Eismann, K. Barnard, and J. Kershenstein, "Design and performance of the civil air patrol archer hyperspectral processing system," *Algorithms and Technologies for Multispectral, Hyperspectral, and Ultraspectral Imagery XI* **5806**(1), pp. 731–742, SPIE, 2005.
2. G. Shaw and D. Manolakis, "Signal processing for hyperspectral image exploitation," *Signal Processing Magazine, IEEE* **19**, pp. 12 –16, jan. 2002.
3. M. Eismann, A. Stocker, and N. Nasrabadi, "Automated hyperspectral cueing for civilian search and rescue," *Proceedings of the IEEE* **97**, pp. 1031 –1055, june 2009.
4. D. Manolakis and G. Shaw, "Detection algorithms for hyperspectral imaging applications," *Signal Processing Magazine, IEEE* **19**, pp. 29 –43, jan. 2002.
5. M. T. Eismann, *Hyperspectral Remote Sensing*, SPIE, Bellingham, Washington, 2012.
6. I. Woodhouse, C. Nichol, P. Sinclair, J. Jack, F. Morsdorf, T. Malthus, and G. Patenaude, "A multispectral canopy lidar demonstrator project," *Geoscience and Remote Sensing Letters, IEEE* **8**, pp. 839 –843, sept. 2011.
7. V. V. Alexander, O. P. Kulkarni, M. Kumar, C. Xia, M. N. Islam, F. L. T. Jr., M. J. Welsh, K. Ke, M. J. Freeman, M. Neelakandan, and A. Chan, "Modulation instability initiated high power all-fiber supercontinuum lasers and their applications," *Optical Fiber Technology* **18**(5), pp. 349 – 374, 2012.
8. D. A. Orchard, A. J. Turner, L. Michaille, and K. R. Ridley, "White light lasers for remote sensing," *Technologies for Optical Countermeasures V* **7115**, pp. 711506–711506–8, SPIE, 2008.
9. Omni Sciences, Inc. `http://www.omnisciinc.com/`.
10. V. V. Alexander, Z. Shi, M. N. Islam, K. Ke, M. J. Freeman, A. Ifarraguerri, J. Meola, A. Absi, J. Leonard, J. Zadnik, A. S. Szalkowski, and G. J. Boer, "Power scalable 25.7w short wave infrared SC laser with near diffraction limited beam and low output variability," in *Conf. on Lasers and Electro-Optics*, 2013. Submitted for Publication.
11. F. L. Pedrotti and L. S. Pedrotti, *Introduction to Optics*, Prentice-Hall, Inc., Englewood Cliffs, New Jersey, 1993.
12. J. T. Verdeyen, *Laser Electronics*, Prentice-Hall, Inc., Englewood Cliffs, New Jersey, third ed., 1995.
13. G. Holst, *CCD Arrays Cameras and Displays*, JCD Publishing, Winter Park, FL, second ed., 1998.
14. A. Berk *et al.*, "MODTRAN4: Radiative transfer modeling for atmospheric correction," *Proc. SPIE* **3756**, pp. 348 – 353, 1999.

Downloaded From: http://proceedings.spiedigitallibrary.org/ on 06/03/2013 Terms of Use: http://spiedl.org/terms